Atmos. Chem. Phys. Discuss., 14, 28757–28807, 2014
www.atmos-chem-phys-discuss.net/14/28757/2014/
doi:10.5194/acpd-14-28757-2014

Atmospheric Chemistry and Physics Discussions

Observations and comparisons of cloud microphysical properties in spring and summertime Arctic stratocumulus during the ACCACIA campaign

G. Lloyd, T. W. Choularton, K. N. Bower, J. Crosier, H. Jones, J. R. Dorsey, M. W. Gallagher, P. Connolly, A. C. R. Kirchgaessner, and T. Lachlan-Cope

Centre for Atmospheric Science, University of Manchester, Manchester, UK

Received: 1 September 2014 – Accepted: 9 October 2014 – Published: 19 November 2014

Correspondence to: G. Lloyd (gary.lloyd@manchester.ac.uk)

Published by Copernicus Publications on behalf of the European Geosciences Union.

Abstract

Measurements from four case studies in spring and summer-time Arctic stratocumulus clouds during the Aerosol–Cloud Coupling And Climate Interactions in the Arctic (ACCACIA) campaign are presented. We compare microphysics observations between cases and with previous measurements made in the Arctic and Antarctic. During ACCACIA, stratocumulus clouds were observed to consist of liquid at cloud tops, often at distinct temperature inversions. The cloud top regions precipitated low concentrations of ice into the cloud below. During the spring cases median ice number concentrations ($\sim 0.5\,L^{-1}$) were found to be lower by about a factor of 5 than observations from the summer campaign ($\sim 3\,L^{-1}$). Cloud layers in the summer spanned a warmer temperature regime than in the spring and enhancement of ice concentrations in these cases was found to be due to secondary ice production through the Hallett–Mossop (H–M) process. Aerosol concentrations during spring ranged from ~ 300–$400\,cm^{-3}$ in one case to lower values of ~ 50–$100\,cm^{-3}$ in the other. The concentration of aerosol with sizes, $D_p > 0.5\,\mu m$, was used in a primary ice nucleus (IN) prediction scheme, DeMott et al. (2010). Predicted IN values varied depending on aerosol measurement periods, but were generally greater than maximum observed median values of ice crystal concentrations in the spring cases, and less than the observed ice concentrations in the summer due to the influence of secondary ice production. Comparison with recent cloud observations in the Antarctic summer (Grosvenor et al., 2012), reveals lower ice concentrations in Antarctic clouds in comparable seasons. An enhancement of ice crystal number concentrations (when compared with predicted IN numbers) was also found in Antarctic stratocumulus clouds spanning the Hallett–Mossop (H–M) temperature zone, but concentrations were about an order of magnitude lower than those observed in the Arctic summer cases, but were similar to the peak values observed in the colder Arctic spring cases, where the H–M mechanism did not operate.

ACPD
14, 28757–28807, 2014

1 Introduction

The Arctic is a region that has experienced rapid climate perturbation in recent decades, with warming rates there being almost twice the global average over the past 100 years (ACIA, 2005; IPCC 2007). The most striking consequence of this warming has been the decline in the extent and area of sea ice, especially in the warm season. The lowest sea ice extent and area on record were both observed on 13 September 2012 (Parkinson and Comiso, 2013) and despite some uncertainty, ice-free Arctic summers could become a reality by 2030 (Overland and Wang, 2013). The underlying warming is very likely caused by increasing anthropogenic greenhouse gases and arctic amplification, which is a well-established feature of global climate models (see for example IPCC 5th Assessment Report 2014). However, the details of Arctic climate are complex with interactions between the atmospheric boundary layer, cloud, overlying sea-ice and water leading to a number of feedback mechanisms. These interactions are not well understood due to variability in the spatial and temporal extent of feedback mechanisms, and the fact that those that are included in Global Climate Models (GCMs) may not be accurately parameterised (Callaghan et al., 2011). Clouds play an important role in a number of proposed feedback processes that may be active in the Arctic (Curry et al., 1996; Walsh et al., 2002), Arctic clouds are the dominant factor controlling the surface energy budget, producing a mostly positive forcing throughout the year, apart from a brief cooling period during the middle of summer (Intrieri et al., 2002a). These clouds affect both the long-wave (year-round) and short-wave (summer-only) radiation budgets, and influence turbulent surface exchange. Cloud microphysical influence on cloud radiative properties depends on the amount of condensed water and the size, phase and habit of the cloud particles (Curry et al., 1996). These factors are controlled in part by the Cloud Condensation Nuclei (CCN) and Ice Nuclei (IN) concentrations and properties. Very low aerosol concentrations in the Arctic can result in clouds with properties differing greatly from those at mid-latitudes (Tjernström et al., 2008). A paucity of observations in the Arctic means that neither the aerosol processes,

ACPD
14, 28757–28807, 2014

nor cloud properties are well understood or accurately represented within models, with the result that aerosol and cloud-forcing of Arctic climate is poorly constrained.

In the Arctic lower troposphere low cloud dominates the variability in Arctic cloud cover (Curry et al., 1996), with temperature and humidity profiles showing a high frequency of one or more temperature inversions (Kahl, 1990) below which stratocumulus clouds form. During the Arctic summer, therefore, these low clouds often consist of multiple layers, with a number of theories describing their vertical separation (Herman and Goody, 1976; Tsay and Jayaweera, 1984; McInnes and Curry, 1995a). Such cloud layers have been observed during different seasons but the relationship between temperature and the formation of ice in them is not well understood. Jayaweera and Ohtake (1973) observed very little ice above −20 °C, but Curry et al. (1997) observed ice to be present in clouds at temperatures between $-8\,^{\circ}\mathrm{C} < T < -14\,^{\circ}\mathrm{C}$ during the Beaufort Arctic Storms Experiment (BASE). It is possible that the large variation in temperature at which glaciation is observed is caused by changes in the concentration and composition of aerosol (Curry, 1995). Recent work, such as in the Arctic Cloud Experiment (ACE) (Uttal et al., 2002) has improved our knowledge of Arctic mixed-phase clouds, which dominate in the coldest 9 months of the Arctic year. ACE reported that clouds were mainly comprised of liquid tops, tended to be very long lived and continually precipitated ice. The longevity of these clouds might be considered unusual as the formation of ice leads to loss of water through the Wegener–Bergeron–Findeison process. More recently the Mixed-Phase Arctic Cloud Experiment (M-PACE, 2004) investigated the Arctic autumn transition season. M-PACE was conducted on the North slope of Alaska, in the area to the east of Barrow (Verlinde et al., 2007). Again predominantly mixed-phase clouds were observed with liquid layers present at temperatures as low as −30 °C. Remote sensing studies also showed that ice was generally present in low concentrations, mostly associated with precipitation shafts, however, there was also evidence of light snow below thicker layer clouds. IN concentrations were also measured and observed to be low, consistent with liquid water being observed down to very low temperatures. Here we present detailed airborne microphysical and aerosol

ACPD
14, 28757–28807, 2014

measurements made in stratocumulus cloud regions in the European Arctic during the recent Aerosol–Cloud Coupling And Climate Interactions in the Arctic (ACCACIA) campaigns. We present data from two aircraft during early spring, in March and April 2013, and from a single aircraft during the following Arctic summer, in July 2013.

The objectives of this paper are:

1. to report the microphysics and cloud particle properties of Arctic clouds, and the properties, number and size distributions of aerosols in the vicinity of these,
2. to identify the origin of the ice phase in these clouds and to compare ice crystal number concentrations with the parameterisation of primary Ice Nucleus (IN) concentrations of DeMott et al. (2010),
3. to compare the cloud physics in spring and summer conditions and to identify any contributions of secondary ice particle production,
4. to compare and contrast the mixed phase cloud microphysics of Arctic clouds with clouds observed in the Antarctic.

2 Methodology

The ACCACIA campaigns took place during March–April 2013 and July 2013. They were conducted in the region between Greenland and Norway mainly in the vicinity of Svalbard (and further afield to the south and west of the archipelago). The overarching theme of the project was to reduce the large uncertainty in the effects of aerosols and clouds on the Arctic surface energy balance and climate. Key to the work presented here is an understanding the microphysical properties of Arctic clouds and their dependence on aerosol properties. To this end the FAAM BAe-146 aircraft performed a number flights incorporating profiled ascents, descents and constant altitude runs below, within and above cloud during the spring period. This provided high-resolution

ACPD
14, 28757–28807, 2014

measurements of the vertical structure of the cloud microphysics and the aerosol properties in and out of cloud regions. The British Antarctic Survey (BAS) Twin Otter aircraft flew during both campaign periods, providing a subset of the BAe-146 measurements. It was the only aircraft present during the summer period. A total of 9 science flights were conducted during the spring period with complementary flights from the BAS twin otter and 6 flights by the BAS twin otter alone during the summer period.

Two case studies are selected from both the early spring and summer campaigns. The spring campaign case studies were selected for having quite different aerosol loadings within the boundary layer. One was in Arctic air with low total aerosol numbers, while the second had higher aerosol loadings in the boundary layer. Summer flight cases were selected for being the cases with higher cloud layer temperatures in comparison to the spring cases. Summer case cloud layer temperatures were significantly higher than in the spring cases, and were observed to be in the temperature zone, $-3\,^{\circ}\mathrm{C}$ to $-9\,^{\circ}\mathrm{C}$, where a powerful mechanism of secondary ice particle production through rime-splintering, the Hallett–Mossop mechansim, (H–M) (Hallett and Mossop, 1974), is known to operate under particular conditions, and so could greatly enhance ice crystal number concentrations. Temperature profiles in the spring cases revealed stratocumulus cloud temperatures generally between $-10\,^{\circ}\mathrm{C} < T < -20\,^{\circ}\mathrm{C}$, outside of the H–M zone.

2.1 Instrumentation

Instrumentation onboard the Facility for Airborne Atmospheric Measurements (FAAM) British Aerospace-146 (BAe-146, or 146) aircraft used for making measurements of the cloud and aerosol microphysics reported in this paper included: the Cloud Imaging Probe models 15 and 100 (CIP-15 and CIP-100, Droplet Measurement Technologies (DMT), Boulder, USA) (Baumgardner et al., 2001), the Cloud Droplet Probe (CDP-100 Version 2, DMT) (Lance et al., 2010) and the Two Dimensional-Stereoscopic Probe (2D-S, Stratton Park Engineering Company Inc. Boulder, USA) (Lawson et al., 2006). The CIP-15 and CIP-100 are optical array shadow probes consisting of 64 element

ACPD
14, 28757–28807, 2014

photodiode arrays providing image resolutions of 15 and 100 µm respectively. The 2D-S is a higher resolution optical array shadow probe which consists of a 128 element photodiode array with image resolution of 10 µm. The CDP measures the liquid droplet size distribution over the particle size range $3 < d_p < 50$ µm. The intensity of forward scattered laser light in the range 4–12° is collected and particle diameter calculated from this information using Mie scattering solutions (Lance et al., 2010).

A Cloud Aerosol Spectrometer (CAS, DMT) and a Passive Cavity Aerosol Spectrometer Probe (PCASP-100X, DMT) were both used to measure aerosol size distributions onboard the 146. The CAS measures particles in the size range $0.51 < d_p < 50$ µm using forward scattered light from single particles in the 4–13° range and backscattered light in the 5–13° range. Particle size can be determined from both the forward and back-scattered light intensity using Mie scattering solutions (Baumgardner et al., 2001). The PCASP is another Optical Particle Counter (OPC) and measures aerosol particles in the size range $0.1 < d_p < 3$ µm. In this instrument, particles are sized through measurement of the intensity of laser light scattered within the 35–120° range (Rosenberg et al., 2012). All the above instruments were mounted externally on the FAAM aircraft. Non refractory aerosol composition measurements were provided using an Aerodyne Compact-Time of Flight Aerosol Mass Spectrometer (C-ToF-AMS) whilst aerosol black carbon measurements were provided by a single particle soot photometer (SP-2, DMT). Results from these will be reported elsewhere. Examples of additional core data measurements that were also used in this paper include temperature (Rosemount/Goodrich type 102 temperature sensors) and altitude measured by the GPS-aided Inertial Navigation system (GIN).

Instrumentation on board the Twin Otter Meteorological Airborne Science Instrumentation (MASIN) aircraft, relevant to measurements reported in this paper included: a CDP-100 for drop size distributions; a 2D-S (summer only), both similar to those on the FAAM aircraft; a CIP-25 (as on FAAM except consisting of a 64 element photodiode array providing an image resolution of 25 µm) and core data including temperature measured by Goodrich Rosemount Probes (models; 102E4AL and 102AU1AG for non-

ACPD
14, 28757–28807, 2014

deiced, and a de-iced temperatures respectively, similar to those used on the FAAM aircraft) and altitude derived from the aircraft avionics (Litef AHRS) system.

2.2 Data analysis

During each science flight measurements of aerosol and cloud microphysical properties were made. The techniques used to interpret these data are described below.

2.2.1 Cloud microphysics measurements

In the paper, 1 Hz data from all cloud and aerosol instruments have been further averaged over 10 s periods for presentation unless peak values, from the 1 Hz data are used, as stated. The different flight profiles and straight and level aerosol and cloud sampling runs for all cases are summarised in Table 1. A main focus of this study is the formation of the ice phase in arctic stratocumulus. Measurements from the 2D-S probe have been presented in preference to other 2D probe data due this probes significantly faster response time (by > a factor of 10), and greater resolution. During the spring cases it was possible to combine 2D-S data with measurements from the CIP-100 to extend the cloud particle size range. Analysis of imagery from these Optical Array Probes (OAPs) was used to calculate number concentrations and discriminate particle phase. Identification of irregular particles, assumed to be ice, was achieved through examination of each particles circularity (Crosier et al., 2011). Ice Water Contents (IWCs) were determined using the Brown and Francis (1995) mass dimensional relationship.

All cloud microphysics probes were fitted with "anti-shatter" tips (Korolev et al., 2011) to mitigate particle shattering on the probe. However, even with these modifications shattering artifacts may still be present, particularly under some cloud conditions and these need to be corrected for (Field et al., 2006). To minimise such artifacts, Inter-Arrival Time (IAT) histograms were analysed in an attempt to identify and remove these additional particles, i.e. by removing particles with very short IATs that are indicative

ACPD
14, 28757–28807, 2014

of shattered ice crystals. Crosier et al. (2013) reported that careful analysis of IAT histograms for different cloud microphysical conditions is needed to determine the most appropriate IAT threshold for best case elimination of such artifacts. For example, in regions of naturally high ice crystal number concentrations, such as in the H–M secondary ice production temperature zone, the minimum IAT threshold may need to be reduced more than is usual so as not to exclude too many naturally generated ice crystals with short IATs. In this study, we found a minimum IAT threshold of 1×10^{-5} and 2×10^{-5} s for the 2D-S and CIP-15 instruments respectively, to be appropriate IAT values for the majority of cloud region data presented.

Measurements of the liquid and ice properties of cloud layers observed during each science flight were binned as a function of altitude and are presented in Figs. 10, 11 and 12. The case descriptions provide information about typical cloud penetrations by the aircraft and describe the dominant microphysical structures observed during each science flight. Additional descriptions of profiles made during each flight can be found in the Appendix.

2.3 Aerosol measurements

In each case study, aerosol concentration measurements were used to calculate the predicted primary ice nuclei (IN) concentrations from the DeMott et al. (2010, hereafter D10) parameterisation of primary ice nuclei numbers, which is dependent on the number concentration of aerosol particles with diameters $> 0.5\,\mu m$. Combined measurements of the aerosol concentration using the PCASP and CAS (for spring), and CAS (for summer), were used from cloud free regions selected by applying maximum Relative Humidity (RH) thresholds. This was done to reduce the contribution of any haze aerosol particles less than 0.5 µm in size growing into the size range at higher humidities and being incorrectly included. The FAAM CAS instrument has a lower size threshold of 0.51 µm. D10 notes that the maximum possible aerosol size that could be measured and included in their D10 parameterization was 1.6 µm. However, due to the size bins utilised by the CAS instrument this upper threshold had to be relaxed

ACPD
14, 28757–28807, 2014

to 2 µm, although the extra contribution to the aerosol concentrations used in the calculations is likely to be small. Grosvenor et al. (2012) demonstrated that the scheme is not particularly sensitive to small changes in total aerosol concentrations > 0.5 µm in clean Antarctic regions. Measurements from the higher resolution PCASP were selected from the size range 0.5 to 1.6 µm, in keeping with the D10 scheme. The D10 predicted IN concentrations were then compared directly as a function of temperature with the observed ice crystal concentrations. The minimum observed median temperature was input to D10 and predicted IN numbers compared with the maximum observed median ice crystal number concentrations (Fig. 11) for the clouds during each of the 4 cases. The results are shown in Table 2.

The results of this comparison from all 4 cases can be compared with previous observations of Arctic clouds and with recent aircraft measurements of clouds over the Antarctic Peninsula in the summer (Grosvenor et al., 2012).

3 Spring case 1 – Friday 22 March 2013 (FAAM flight B761)

On this day the FAAM aircraft first flew from Kiruna, Sweden (67.85° N, 20.21° E) to Svalbard, Norway landing at Longyearbyen, (78.22° N, 15.65° E) to refuel. After take-off at ~ 11:45 UTC a ~ 2 h science flight was undertaken to the south east of Svalbard (Fig. 1a) before returning to Kiruna. The objective was to investigate stratocumulus cloud in this area, near to the ice edge, and from over ice to open ocean (moving from N to S in the target area). The flight focused on a series of profiled descents and ascents to enable measurements to be made of the cloud layer from below cloud base to above cloud top and into the inversion layer above. During the flight there were 3 significant penetrations through the inversion at cloud top and in each case there was a marked temperature increase of ~ 5 °C. Microphysical time series data for this case are presented, with the relevant runs highlighted in Fig. 2. A description of one cloud profile is given here, with further profiles described in Appendix A. For this case, boundary layer aerosol number concentrations (from the PCASP) were found to be

ACPD
14, 28757–28807, 2014

relatively low at ∼ 50–100 cm^{-3}. Widespread low cloud was observed south and east of Svalbard (Fig. 1) with winds from the north advecting from over the sea-ice towards open sea. Earlier dropsonde measurements (on the transit into Longyearbyen prior to refuelling) showed surface winds of ∼ 3 m s^{-1} increasing to 15 m s^{-1} at 500 mbar.

3.1 Profiled descent A1

During profile A1 the aircraft (now travelling north) descended from the inversion layer. Cloud top was encountered at 1650 m (T = −18.6 °C). The highest values of N_{ice} were observed in the cloud top region, at ∼ 4 L^{-1} with peaks up to 7 L^{-1} where IWCs were 0.15 g m^{-3}. Particles here consisted of small irregular ice particles (mean size ∼ 360 µm) that showed evidence of riming, together with small droplets. CDP LWC increased to 0.3 g m^3 with N_{drop} ∼ 55 cm^{-3} (mean diameter ∼ 17 µm). At an altitude of around 1400 m a.s.l. (∼ 250 m below cloud top) N_{ice} decreased to ∼ 1 L^{-1}, and mean ice particle size increased to ∼ 395 µm. N_{drop} increased to ∼ 70 cm^{-3}, while mean size decreased slightly (∼ 16 µm). LWCs generally decreased somewhat to ∼ 0.2 g m^{-3}. As the aircraft descended to an altitude of ∼ 1150 m, N_{ice} increased by approximately a factor of 2 (to ∼ 2 L^{-1}). At around 13:15 UTC a number of rapid transitions from liquid to predominantly glaciated conditions were observed in the mid cloud region at 730 m and T = −12 °C. The initial phase change occurred as LWC decreased from 0.2 to 0.01 g m^{-3} while IWCs increased to a peak value of 0.2 g m^{-3} and peak N_{drop} fell close to 1 cm^{-3}. 2D-S imagery (Fig. 3c) highlights these changes taking place as small droplets are quickly replaced by small irregular ice crystals and eventually larger snow particles (mean diameter ∼ 610 µm) that consisted of heavily rimed ice crystals and aggregates, some of which can be identified as exhibiting a dendritic habit. Observations of dendritic ice are consistent with the ice crystal growth habit expected at this temperature level (−12 °C). Three further swift phase transitions were observed as the aircraft approached cloud base. LWC in the liquid dominated regions was between ∼ 0.15 and

ACPD
14, 28757–28807, 2014

0.25 g m^{-3} while N_{drop} peaked at ~ 130 cm^{-3}. During the ice phase sections of the transition cycle, mean particle sizes were ~ 615 µm and N_{ice} peaked at up to 5 L^{-1}. The contribution of these glaciated cloud regions to the IWC was considerable, with values up to 0.1 g m^{-3} recorded. These transitions ended as the aircraft descended below cloud base (T = −12 °C) at 700 m a.s.l., and precipitating snow was observed (mean size ~ 710 µm).

4 Spring case 2 – Wednesday 3 April 2013 (FAAM flight B768)

The FAAM aircraft departed Longyearbyen at around 11:00 UTC and conducted measurements to the NW of Svalbard to investigate low-level clouds over sea ice as well as the transition to deeper more convective type cloud as the aircraft moved away from the ice edge and over warmer water (moving from NW to SE in the target area – Fig. 1b). A low pressure (1004 mbar) region was centred south of Svalbard with an associated band of cloud and precipitation. To the NW of Svalbard, within the measurement area, surface winds were E–NE and < 10 m s^{-1}. Measurements revealed an airmass containing significantly more aerosol than in Spring case 1, with PCASP concentrations typically ~ 300–400 cm^{-3} in the boundary layer. During the flight the aircraft made two distinct saw tooth profiles through the cloud layer and into the inversion above cloud top where temperatures in each instance increased by ~ 2 °C. Figure 4 shows time series of the microphysical measurements made during this science flight. Further profile descriptions can be found in Appendix B.

4.1 Profiled descent B1

Flying NW, the aircraft performed a profiled descent from the inversion layer (T = −16.5 °C) into cloud top, ~ 1550 m a.s.l., where the measured temperature was −17 °C. LWCs rose to a peak value of ~ 0.9 g m^{-3} and N_{drop} (mean diameter ~ 15 µm) peaked at ~ 320 cm^{-3}. The highest values of N_{ice} never exceeded 0.5 L^{-1} in this cloud top re-

ACPD
14, 28757–28807, 2014

gion and imagery from the 2D-S probe revealed many small droplets with isolated small (mean size ∼ 223 µm) irregular ice crystals (Fig. 5a). After descending through this brief cloud top region N_{ice} increased to ∼ 0.5 L^{-1}. As the aircraft descended over the next 500 m mean droplet concentrations gradually increased from 300 to 370 cm^{-3} with mean diameters decreasing slightly to 12.5 µm. LWCs fell from 0.7 to 0.2 $g\,m^{-3}$ over the same period and temperatures increased from −17.5 °C to −13.5 °C. N_{ice} values remained fairly constant and IWCs peaked around ∼ 0.5 $g\,m^{-3}$. 2D-S imagery showed ice crystals (mean diameter 295 µm) to be mainly dendritic in nature. During the last 160 m depth of the cloud before cloud base, N_{ice} remained similar to the mid-cloud region. However, concentrations of liquid droplets measured by the CDP showed greater variability. Peaks in number concentrations reached as high as 430 cm^{-3}, with rapid changes down to as low as 110 cm^{-3}.

The aircraft passed cloud base at 700 m a.s.l. encountering low concentrations (< 0.5 L^{-1}) of precipitating snow. Interestingly, as the aircraft continued its descent (to 50 m a.s.l.) a significant increase in N_{ice} was observed (T = −9 °C), with 10 s mean values of 2 L^{-1} and 1 s peak values of 4 L^{-1}. Images from the 2D-S revealed (Fig. 5d) snow precipitation co-existing with small columnar ice crystals. CDP LWC was very low, < 0.01 $g\,m^{-3}$, however examination of the 2D-S imagery showed the presence of spherical drizzle droplets, larger than the maximum detectable size of the CDP. Size distribution data from the 2D-S in this region revealed an additional mode dominated by these smaller columnar ice crystals, typically 80 µm in size. As the aircraft ascended again, these higher concentrations of ice crystals diminished before cloud base was reached again at ∼ 850 m a.s.l.

5 Summer case 1 – Tuesday 18 July 2013 (flight number M191)

The BAS Twin Otter aircraft departed Longyearbyen airport at ∼ 07:00 UTC to conduct a ∼ 2 h science flight to the North of Svalbard (Fig. 1c). Extensive low cloud was present in the area with light winds < 5 $m\,s^{-1}$ from the North. The objectives of the flight were to

ACPD
14, 28757–28807, 2014

measure aerosol concentrations and composition in the vicinity of cloud, together with the microphysical properties of the clouds by undertaking a combination of profiles and straight and level runs through stratocumulus cloud layers to capture the microphysical structure. Time series of data collected during this flight are presented in Fig. 6. Profile C2 is described below, with details of the measurements made during C1 found in Appendix C.

5.1 Profile C2

The aircraft performed a sawtooth profile, descending from cloud top at ~ 3300 m down to a minimum altitude of ~ 2300 m followed by a profiled ascent to complete the sawtooth. During the descent into cloud top (T = −9 °C) LWCs rose sharply to peak values of 0.3 g m^{-3} and N_{drop} (mean diameter 19 µm) increased to 155 cm^{-3}. N_{ice} in the cloud top regions peaked at 1 L^{-1}. With decreasing altitude, LWC declined gradually to values close to 0.01 g m^{-3}. As the temperature increased to above −8 °C, ice crystal number concentrations (mean diameter 210 µm) increased to 5 L^{-1}, with peaks to ~ 12 L^{-1}. 2D-S imagery revealed the presence of small columnar ice crystals together with small liquid droplets (CDP mean diameter 8.5 µm) and some irregular ice particles. At 2880 m (T = −6.5 °C) the cloud dissipated until the next cloud layer was encountered 200 m below (T = −5 °C). In this region CDP LWC and N_{drop} were more variable than in the cloud layer above. Generally LWCs were < 0.1 g m^{-3} with peaks in N_{drop} to ~ 155 cm^{-3} and transitions between liquid cloud and predominantly glaciated cloud were observed. N_{ice} peaked at 25 L^{-1} and IWCs peaked at 0.15 g m^{-3}. 2D-S imagery showed many columnar ice crystals, typical of the growth regime at this temperature (~ −5 °C) and consistent with the enhancement of N_{ice} through the H–M process. The aircraft reached its minimum altitude (T = −3 °C) before beginning a profiled ascent to complete the sawtooth. The cloud microphysics of the lower cloud layer were the same as encountered in the descent leg, but with LWCs at times higher (peaks up to 0.2 g m^{-3}). Transitions between liquid and glaciated phases were observed again, with a notable period of high

ACPD
14, 28757–28807, 2014

N_{ice}(T = −4 °C), peaking at ∼ 35 L^{-1} and with IWCs as high as 0.3 g m^{-3}. 2D-S images again revealed many columnar ice crystals (mean diameter 295 µm), some of which had aggregated, together with irregular ice crystals and liquid droplets. At 2770 m CDP measurements again indicated the presence of a cloud free layer, but over a reduced vertical extent of 100 m, about half the depth observed in the earlier descent. In this region N_{ice} reached 8 L^{-1} in the presence of larger drizzle droplets (Fig. 7d). Temperatures in the region were around −4 °C. Images from the2D-S showed the presence of small irregular ice crystals with columnar habits. The higher cloud layer cloud base was penetrated at ∼ 2870 m, and N_{drop} increased rapidly to 75 cm^{-3}, while LWCs increased gradually to peak values of 0.25 g m^{-3} at cloud top (T =∼ −6 °C). N_{ice} values were lower than those observed lower in the cloud and generally below 5 L^{-1}. Images of the particles showed the presence of small droplets (CDP mean diameter 18 µm) together with small irregular ice crystals (mean diameter 115 µm).

6 Summer case 2 – Wednesday 19 July 2013 (M192)

The BAS aircraft departed Longyearbyen at ∼ 09:00 UTC intending to investigate cloud microphysics and aerosol properties to the north of Svalbard (Fig. 1d). On arrival in the observation area the forecasted cloud was not present so the flight was diverted to the south east of Svalbard to meet an approaching cloud system. Surface pressure charts showed a low pressure system over Scandinavia (central pressure 1002 mbar), with a warm front south east of Svalbard that was moving north west. Surface winds in this area were ∼ 13 m s^{-1} from the north east. In-situ cloud microphysics measurements were made for approximately 1.5 h in total. To meet the objectives of the flight straight and level runs and saw tooth profiles were performed through the cloud layers. Microphysics time series data from the flight are shown in Fig. 8. Profile D2 is described below, with additional profile D1 discussed in Appendix D.

ACPD
14, 28757–28807, 2014

6.1 Profile D2

During period D1, the aircraft also performed a number of straight and level runs combined with sawtooth profiles to capture the microphysical structure of the cloud layers present. At 3100 m the aircraft flew a straight and level run below cloud base and encountered a region of snow precipitation at temperatures between −2 °C and − 3 °C. N_{ice} peaked at 5 L^{-1} giving peaks in calculated IWCs of ∼ 0.1 g m^{-3}. Probe imagery showed ice crystals (mean diameter 410 µm) dominated by irregular particles, with some evidence of plate like and dendritic structures. During a subsequent profiled ascent up to 3400 m (to begin an extended SLR) the aircraft penetrated cloud base at 3300 m (T = −4 °C). By the top of the ascent LWCs rose to ∼ 0.1 g m^{-3} with N_{drop} generally observed to be between 10 and 50 cm^{-3} (mean diameter 12 µm). N_{ice} in this region was between 0 and 1 L^{-1} with peaks to 3 L^{-1} and particles consisted of irregular ice particles, columnar ice and small liquid droplets. The mean diameter of the ice particles in this region was 470 µm. Continuing at 3400 m altitude, the aircraft encountered a break in the cloud layer that lasted for around 1 min (∼ 6 km), before a subsequent cloud layer was observed that had similar LWCs to the previous cloud layer (∼ 0.1 g m^{-3}) but with generally lower droplet concentrations (of mean diameter 17.5 µm); with mean N_{drop} values of 15–30 cm^{-3}. N_{ice} values in this region were lower than before (< 0.5 L^{-1}). The sampling of this cloudy region was brief before another gap in cloud was observed that lasted ∼ 2 min. The end of this second clear region was defined by a sudden transition to columnar ice and small irregular particles (mean diameter 410 µm) in concentrations up to a peak of 4 L^{-1}. This region was mostly glaciated with LWC < 0.01 g m^{-3}. During this SLR there were very swift transitions observed between predominantly glaciated regions containing ice crystals (peaking at 4 L^{-1}) of a columnar nature, and then mainly liquid regions consisting of low concentrations (< 30 cm^{-3}) of small liquid droplets (mean diameter 14 µm) and LWCs (∼ 0.01 g m^{-3}) (Fig. 9c and d). This predominantly glaciated period ended when the aircraft performed a profiled ascent and N_{ice} decreased to < 0.5 L^{-1} while LWCs increased to a peak of

ACPD
14, 28757–28807, 2014

0.3 g m^{-3} and N_{drop} rose to a maximum of ∼ 120 cm^{-3} (mean diameter 14 µm). The aircraft penetrated cloud top at 3700 m (T = −4.5 °C).

After climbing above cloud top, the aircraft performed a profiled descent back into the cloud layer to begin another SLR at 3400 m (T = −4.5 °C). At cloud top LWCs were ∼ 0.2 g m^{-3} N_{drop} peaked at 115 cm^{-3}. N_{ice} values were greater than in the previous cloud top region. There were two peaks of up to 15 L^{-1} with particle mean particle diameters of ∼ 370 µm. Images show columnar particles, some of which had aggregated, were present together with small liquid droplets (CDP mean diameter 11.5 µm). The second peak contained columnar ice crystals of a similar size (mean diameter 400 µm). The largest spike in ice concentrations occurred in close proximity to the first peak, with values as high as 20 L^{-1} observed, while IWCs peaked at 0.15 g m^{-3}. Images showed irregular and columnar ice particles (mean diameter 260 µm) present together with small liquid droplets (CDP mean diameter 12 µm) (Fig. 9b). After these highs in ice number, concentrations declined to ∼ 2.5 L^{-1} before the aircraft made a short profiled ascent and concentrations rose again to peak values of 10 L^{-1}. At 3550 m cloud dissipated and the aircraft descended through a predominantly clear region before reaching another significant cloud layer at 3450 m (T = −4 °C). CDP N_{drop} and LWCs were variable in this region with 10 s mean values rising to 145 cm^{-3} and 0.1 g m^{-3} respectively. The droplets were small (mean diameter 8 µm) and ice was almost completely absent during this part of the profile. After an SLR at 3400 m, the aircraft descended as the cloud layer dissipated but encountered another, more significant layer around 3250 m (T = −2.5 °C). LWCs increased to peak values of 0.4 g m^{-3} and droplet concentrations (mean diameter 10.5 µm) increased to a peak of 410 cm^{-3}. This cloud layer was again predominantly liquid. A spike in 2D-S concentrations was observed which imagery revealed was again due to drizzle droplets. These date were removed from the ice dataset.

ACPD
14, 28757–28807, 2014

7 Primary IN parameterization comparison

Ice number concentrations as a function of altitude for science flight periods have been presented and here these observations are compared to calculations of the primary IN concentrations predicted using the D10 scheme, using aerosol concentrations (diameter $> 0.5\,\mu m$) that were measured on each flight as input. DeMott et al. (2010) analysed datasets of IN concentrations over a 14 year period from a number of different locations and found that these could be related to temperature and the number of aerosol $> 0.5\,\mu m$. The parameterisation provided an improved fit to the datasets and predicted 62 % of the observations to within a factor of 2. Table 2 shows mean aerosol concentrations for measurement periods during each case, the input temperature to D10, the maximum median ice concentration used for comparison and the predicted IN concentration based on both the PCASP and CAS aerosol measurements (where available). During the spring measurement campaign it was possible to compare the CAS and PCASP probe data sets. Despite some variation in concentrations reported between the two instruments, D10 predicted IN values were found to be fairly insensitive to these differences. Grosvenor et al. (2012) highlighted that changes of about a factor of 4 produced a very limited change in the IN concentrations predicted by the scheme.

In spring case 1 the maximum median ice value reached $0.61\,L^{-1}$ so predicted IN values were generally higher (between a factor of 2 and 4) than this median ice concentration observation. However peaks in ice concentrations of up to $\sim 10\,L^{-1}$, were also observed (Fig. 2) so on these occasions D10 significantly under predicts observed ice number concentrations when compared to these peak values. During spring case 2, maximum median ice concentration values were similar to spring case 1. Secondary ice production was observed close to the sea surface in this case so these higher median concentrations have been disregarded for the purposes of the D10 primary IN comparison. Aerosol measurements from the CAS were lower than from the PCASP but predicted IN values were in good agreement (less than a factor of 2) with the ob-

ACPD
14, 28757–28807, 2014

served maximum median concentration. The peak concentrations observed during the flight were $\sim 5\,L^{-1}$ (Fig. 4) and as in the first spring case D10 under predicted these peak concentrations by about a factor of 10.

During summer case 1 the minimum cloud temperatures were higher ($T = -10\,^{\circ}C$) than in the spring cases. Maximum median ice concentrations observed were also higher ($3.35\,L^{-1}$). The origin of these enhanced concentrations is attributed to SIP, making a direct comparison with the D10 primary IN scheme difficult. Predicted IN concentrations from D10 were found to underestimate the maximum median ice concentrations observed in this summer case (due to secondary ice production), but were in agreement with the concentrations observed near cloud top, where the ice phase is likely to represent primary heterogeneous ice nucleation. Observed ice concentrations in summer case 2 were also higher than in the previous spring cases and similar to the first summer case. The second case had higher minimum cloud temperatures than in the first summer case ($T = -4.3\,^{\circ}C$). Due to effect of SIP at this temperature, it was not possible to compare D10 with the concentrations of ice observed in these clouds.

8 Discussion

Summaries of typical profiles during each case have been presented, with microphysics data encompassing all cloud penetrations during the science flights presented as a function of altitude shown in Figs. 10, 11 and 12. Figure 10 shows the cloud liquid droplet parameters, Fig. 11 the ice crystal concentration statistics and Fig. 12 the ice mass and diameter parameters. In each case (a) is spring case 1, (b) spring case 2, (c) summer case 1 and (d) summer case 2. The yellow lines on the ice plots (Fig. 8) show the approximate location of cloud top and cloud base altitudes deduced from liquid water content measurements exceeding $0.01\,g\,m^{-3}$ from the CDP. It is notable that droplet concentrations (Fig. 10) are much higher in the second spring case than in the first spring case (max median values ~ 60 and $\sim 400\,cm^{-3}$ for spring case 1 and 2 respectively) and this is attributed to differences in aerosol concentrations. N_{drop} are

ACPD
14, 28757–28807, 2014

similar in the two summer cases (max median values 100–150 cm^{-3}) and lie between the two spring cases.

During the spring cases the mixed phase cloud layers were found to be approximately adiabatic and exhibited generally uniform increases in LWC and droplet diameter (Fig. 10) to liquid cloud tops that were observed to precipitate ice. At and above cloud top, well-defined temperature inversions were present. The ice phase is very likely to have been initiated through primary heterogeneous ice nucleation in the temperature range spanned by these clouds (approximately $-10\,^{\circ}C > T > -20\,^{\circ}C$). Generally low concentrations of ice crystals were observed (max median value 0.61 L^{-1}) (Table 2), but with peaks up to ~ 5–10 L^{-1} in both spring cases (Fig. 11). Cloud top regions consisted of small liquid droplets (median diameter ~ 15 and 25 µm for spring cases 1 and 2 respectively) (Fig. 10a and b), together with small irregular ice crystals (Figs. 3a and 5a). In both of these cases, ice crystal diameter increased to maximum values of 530 and 660 µm respectively (Fig. 12a and b). The variability in ice crystal diameter (Fig. 12a and b) shows periods where maximum ice crystal diameters increased to ~ 2 mm. These crystals were often comprised of a mixture of large rimed irregular particles (Figs. 3 and 5) and dendritic snow crystals. Median IWC values in the spring cases reached ~ 0.01 $g\,m^{-3}$ (Fig. 12a and b), with peak values during case 1 up to ~ 0.3 $g\,m^{-3}$ compared with 0.1 $g\,m^{-3}$ in case 2. The highest Median LWCs (Fig. 10) were observed at cloud top during spring cases, peaking at 0.3 and 0.5 $g\,m^{-3}$ during cases 1 and 2 respectively. While these clouds were seen to be fairly uniform, time series data (Figs. 2 and 4) show some of the variability in the microphysics that was observed during the science flight.

During the summer cases, the cloud layers spanned a higher temperature range ($-10\,^{\circ}C < T < 0\,^{\circ}C$) and well-defined temperature inversions at cloud top were less evident. There was a much greater tendency towards there being multiple cloud layers that were shallower and less well coupled. During summer case 2 a significant temperature inversion was observed (Fig. 10d) in the cloud base region, which suggested a de-coupling of the boundary layer and the cloud system above. Liquid cloud top

ACPD
14, 28757–28807, 2014

regions with few (generally $< 1\,L^{-1}$) ice crystals, formed through heterogeneous ice nucleation at these temperatures, were observed in both cases (Fig. 11c and d). LWCs in summer case 1 were lower than the spring cases (median values $<\sim 0.1\,g\,m^{-3}$) and similar in shape to the uniform profiles seen in the spring cases. The second summer case had higher median LWCs (up to $0.35\,g\,m^{-3}$) and showed much more variability with a number of increases and decreases in median LWC values with altitude (Fig. 10d). Median cloud top ice concentrations in summer case 1 were similar to the spring cases ($\sim 0.2\,L^{-1}$) (Fig. 11d), however maximum median values lower down in the cloud reached $3.35\,L^{-1}$ (Table 2), about a factor of 14 higher than in the spring cases. Peaks in ice number concentrations around the −5 °C level reached between 30–40 L^{-1}. During the summer, the clouds spanned the temperature range −3 to −8 °C, where a well-known mechanism of secondary ice production operates through splintering during riming; the Hallet–Mossopp process (H–M). The observations in this case, of liquid water together with ice particles at temperatures around −5 °C, are consistent with this process being active and enhancing ice number concentrations (Figs. 7 and 9). Time series (Figs. 6 and 8) showed more variation than in the spring cases. Distinct liquid cloud tops were still evident, but at lower altitudes significant variations in LWCs, droplet number concentrations and ice number concentrations were seen together with gap regions where little or no cloud was present. On a number of occasions predominantly liquid conditions were swiftly replaced by regions of high concentrations of columnar ice crystals. Some of these transitions took place over ∼ 1 s or horizontal distance of the order 60 m. These rapid fluctuations were attributed to the contributions from the H–M process. The process of glaciation through secondary enhancement of ice number concentrations is likely to have caused some of this increased variability in cloud properties too, with liquid droplets quickly being removed through depletion of liquid water by the ice phase. The cloud layers during summer case 2 spanned a higher temperature range than summer case 1. Cloud tops were around −4 °C, and median ice number concentrations reached maximum values of $2.5\,L^{-1}$, about an order of magnitude higher than in the spring cases. Time series (Fig. 8) and percentile

ACPD
14, 28757–28807, 2014

plots (Fig. 11d) showed peaks in ice number concentrations to $\sim 25\,L^{-1}$ and in these regions probe imagery revealed distinctive columnar ice crystals likely to have grown from splinters produced via H–M, into habits typical of growth at these temperatures around −4 °C. In addition, the formation of high ice concentrations may have led to the dissipation of some liquid cloud regions below cloud top due to consumption of the liquid phase by ice crystals growing by vapour diffusion (i.e. ice crystal growth via the Bergeron–Findeisen (B-F) process (Bergeron, 1935). This is consistent with the observed summer clouds being more broken than the clouds observed during spring. However, as discussed in the introduction, it is also recognised that cloud-radiation interactions may lead to the separation of cloud layers during the Arctic summer.

Comparison of the observed N_{ice} with the D10 parameterization of primary ice nuclei numbers revealed that during the spring case 1, maximum median N_{ice} was lower than the primary IN concentrations predicted by D10, but similar in spring case 2. Peaks in N_{ice} were much higher than the D10 IN predictions, by an amount depending on the aerosol measurement period used as input to D10 (Table 2). In the summer cases the enhancement of N_{ice} through the H–M process made a realistic comparison difficult. Despite this difficulty, the first summer case had cloud top temperatures that were just outside the H–M temperature zone (−10 °C) and median N_{ice} in this region was $\sim 0.2\,L^{-1}$, which is within a factor of 2 of values predicted by D10 (Table 2). At lower altitudes the increase in cloud temperatures allowed rime-splintering to enhance concentrations to above what would be expected via primary heterogeneous ice nucleation. In the second summer case cloud top temperatures were higher (−4 °C), and enhancement of the ice crystal number concentrations through SIP prevented observations of any first ice by primary nucleation being made. Ice crystal number concentrations were thus enhanced to values above what was predicted by D10 throughout the depth of the cloud. Whilst primary ice nucleation is identified as the most important ice forming process in the spring clouds, the summer stratocumulus ice concentrations were dominated by secondary ice production via the H–M process as discussed. Due to this SIP

ACPD
14, 28757–28807, 2014

enhancement, ice concentrations in summer reached much higher values than those observed anywhere in the spring cases.

The microphysical structure of the spring and summer stratocumulus layers was found to be consistent with previous observations of arctic clouds. We observed generally low droplet number concentrations with increased concentrations during incursions of higher aerosol loadings. This is consistent with observations by Verlinde et al. (2007). During spring cases, LWCs and liquid droplet size increased uniformly to cloud top, however during summer months the vertical structure of cloud layers was more variable (e.g. Hobbs and Rangno, 1998). During spring cases in particular, liquid cloud tops at distinct temperature inversions continually precipitated low concentrations of ice into the cloud below, which has been observed previously in the Arctic. During the Arctic summer, Hobbs and Rangno (1998) observed generally higher ice concentrations with columnar and needle ice crystals in concentrations of "tens per litre" where stratocumulus cloud top temperatures were between −4 and −9 °C. The summer cases we observed contained median values of N_{ice} that were 4–6 times greater than we observed in the spring cases. In the spring, the cloud layers were colder than the temperature range within which H–M is active, and accordingly contained peak concentrations of ice closer to predictions from D10. In the summer cases, the clouds spanned a warmer temperature range between about 0 and −10 °C, leading to low concentrations of primary ice that when conditions became suitable, were then enhanced through rime-splintering. During the spring we also observed cloud that penetrated into the inversion layer, rather than being capped below it. On average the cloud top was seen to extend ∼ 30 m into the inversion layer over which range the mean temperature increase was ∼ 1.6 °C.

Changes in aerosol concentrations and composition have been suggested as a possible factor in explaining previous observations of the glaciation of arctic clouds at different temperatures (Curry et al., 1996). During spring case 2 higher concentrations of aerosol were observed when compared to spring case 1. Droplet number concentrations were also much higher in spring case 2, generally 300–400 cm^{-3} in comparison

ACPD
14, 28757–28807, 2014

to spring case 1 where concentrations were generally ∼ 50–100 cm^{-3}. Despite this, no significant difference was observed in the ice number concentrations. However, it should be noted that despite the higher total concentrations, the population of aerosol > 0.5 µm was not significantly enriched in spring case 2 compared to the spring case 1. D10 has a dependency only on this portion of the aerosol size distribution, so may explain the similar primary ice number concentrations for both spring case studies.

Grosvenor et al. (2012) studied stratocumulus clouds in the Antarctic over the Larsen C ice shelf. These observations contained periods where temperatures were comparable to those in the spring cases studied here. The lower layers of Antarctic cloud were also reported to contain higher concentrations of ice produced via the H–M process, similar to the summer cases that we have discussed. A summary of some of the measurements reported from the Antarctic in Grosvenor et al. (2012) can be found in Table 3. Measurements of cloud regions outside the H–M temperature zone revealed very low ice number concentrations, with maximum values about 2 orders of magnitude lower than those observed in the spring cases reported here. Aerosol concentrations from a CAS probe (similar to the one deployed in this study) reported generally lower concentrations of aerosol particles D_p > 0.5 µm. The D10 IN predictions in the Antarctic were reported to compare better with maximum, rather than mean ice values. A similar result was found in this study where predicted primary IN values were greater than observed median values. However, when comparing with peak ice concentration values the scheme significantly under-predicted these. Grosvener et al. (2012) discussed the possibility that due to the D10 parameterisation being based on mean IN concentrations from many samples, the finding that IN predictions compared well with the maximum values rather than mean values may suggest the scheme was over predicting IN concentrations generally in the Antarctic (for these particular cases at least). In the H–M layer in the Antarctic over Larsen C, ice crystal number concentrations were found to be higher than those observed in colder temperature regimes (not spanning the H–M temperature range), in keeping with the findings from the Arctic presented this paper. However the concentrations produced by the H–M process in the Antarctic were

ACPD
14, 28757–28807, 2014

generally only a few per litre, approximately an order of magnitude lower than those observed during the summer cases in the Arctic.

9 Conclusions

Detailed microphysics measurements made in Arctic stratocumulus cloud layers during the early spring and summer, have been presented.

- Two spring and two summer cases were presented. The cloud layers during summer cases spanned a warmer temperature range ($\sim 0\,^{\circ}\mathrm{C} \geq T > -10\,^{\circ}\mathrm{C}$) than in spring (generally $\sim -10\,^{\circ}\mathrm{C} \geq T > -20\,^{\circ}\mathrm{C}$).
- Spring case 2 had significantly higher aerosol concentrations (~ 300–$400\,\mathrm{cm}^{-3}$) compared to the first spring case (~ 50–$100\,\mathrm{cm}^{-3}$). Despite this difference, ice number concentrations were found to be similar in both spring cases, suggesting the source of the increased aerosol concentrations was not providing additional IN that were efficient over the temperature range $-10\,^{\circ}\mathrm{C} > T > -20\,^{\circ}\mathrm{C}$.
- In the spring cases, cloud layers appeared more uniform with steady increases in LWC and cloud droplet size to cloud top, where low concentrations ($< 1\,\mathrm{L}^{-1}$) of ice were frequently observed to precipitate through the depth of the cloud layer. The small irregular particles observed at cloud top grew to a median diameter $\sim 500\,\mu\mathrm{m}$ in both cases with peaks in diameter $> 1000\,\mu\mathrm{m}$ as the crystals descended through the cloud. 2D-S imagery revealed the dominant growth habit to be dendritic in nature. The summer cases consisted of multiple cloud layers that were observed to be more variable than in the spring. However, liquid cloud top regions were still evident and ice was again observed to precipitate into the cloud layers below.
- The maximum median ice number concentrations observed within cloud layers during the summer cases were approximately a factor of 5 (or more) higher than in

ACPD
14, 28757–28807, 2014

the spring cases. This enhancement in the ice number concentrations is attributed to the contribution of secondary ice production through the H–M process.

– This finding suggests that low level summer stratocumulus clouds situated in the H–M temperature zone in the Arctic may contain significantly higher ice number concentrations than in spring clouds due to the temperature range of the former spanning the active H–M temperature zone.

– Predicted values from the DeMott et al. (2010) scheme of primary ice nuclei, using aerosol measurements obtained during the science flights as input, tended to overpredict IN concentrations compared to the observed maximum median ice crystal number concentrations during the spring, but under-predict IN when compared to peak ice crystal concentrations. During the summer cases, due to contributions from secondary ice production, the scheme predicted significantly lower values of ice particles than those observed.

– Grosvenor et al. (2012) observed lower concentrations of aerosol $> 0.5\,\mu m$ in the Antarctic when compared to similar measurements made in the Arctic. They found that IN predictions using D10 agreed better with their observed peak ice concentration values rather than their maximum mean values. They measured approximately an order of magnitude lower primary ice concentrations in summer Antarctic clouds than in our spring Arctic cases, but did observe enhancement through SIP in warmer cloud layers where concentrations increased to a few per litre. These were still about an order of magnitude less than the enhanced concentrations observed in the Arctic summer cases presented here, but were similar to the peak values observed in spring cases over the Arctic (where no SIP was observed).

ACPD
14, 28757–28807, 2014

Appendix A:

A1 Profiled ascent A1

During profile A1 the aircraft (travelling south) made a profiled ascent from 300 m above the sea surface, reaching cloud base at 650 m, identified using a Liquid Water Content threshold of LWC $> 0.01\,g\,m^{-3}$, as derived from CDP data. Below cloud base the 2D-S probe revealed low concentrations ($< 0.5\,L^{-1}$) of irregular snow (Fig. 3d) particles (mean size $\sim 530\,\mu m$) that had precipitated from the cloud layer above. As the aircraft climbed through cloud base, temperatures decreased to $-11\,^{\circ}C$. CDP droplet concentrations (N_{drop}) (10 s averaged values) increased to $\sim 80\,cm^{-3}$, LWCs peaked at $\sim 0.2\,g\,m^{-3}$ and mean droplet diameters were $\sim 8\,\mu m$. Measurements from the 2D-S showed ice crystals with mean size $\sim 415\,\mu m$ in low concentrations, $\sim 1\,L^{-1}$. Images from the 2D-S revealed irregular snow particles with some dendritic habits coexisting with small liquid droplets. As the ascent continued the aircraft encountered a layer containing higher N_{ice} at $-14\,^{\circ}C$. Ice crystals consisted of snow particles (mean size $350\,\mu m$) in concentrations $\sim 4\,L^{-1}$. Probe imagery showed these to be a mixture of large irregular ice crystals, small, more pristine plate-like crystals and some crystals with columnar habits. The highest 10 s mean N_{ice}, reached $\sim 6\,L^{-1}$ with peak values $\sim 15\,L^{-1}$. These were observed in a region approximately 500 m below cloud top. Maximum 10 s averaged Ice Water Content (IWC) reached $0.2\,g\,m^{-3}$ with peaks up to $0.3\,g\,m^{-3}$ in the same region. Particle images here revealed (Fig. 3b) irregular ice crystals together with a few smaller pristine plates. The mid region of this stratocumulus deck also consisted of liquid droplets (mean diameter $\sim 13\,\mu m$) in concentrations $\sim 75\,cm^{-3}$, and LWC $\sim 0.3\,g\,m^{-3}$, with some 1 s integration periods being as high as $0.5\,g\,m^{-3}$. As the aircraft approached cloud top, where the lowest temperature recorded was $-19.5\,^{\circ}C$, N_{ice} reduced to $\sim 0.5\,L^{-1}$ with mean sizes of $285\,\mu m$, however this region was dominated by liquid droplets (mean diameter $17\,\mu m$) with N_{drop} up to $95\,cm^{-3}$, and LWC values peaking at $0.7\,g\,m^{-3}$. Imagery from the 2D-S revealed many small

ACPD
14, 28757–28807, 2014

droplets together with numerous small irregular ice crystals in this cloud top region. After measuring the vertical structure of the cloud layer, which was approximately 1 km in depth, the aircraft penetrated cloud top at 1675 m and passed through an inversion layer where the temperature increased to −13 °C.

A2 Profiled descent A3

Following another ascent, the aircraft performed a profiled descent (A3) from the inversion layer, $T = -13\,^{\circ}\mathrm{C}$, penetrating cloud top at 1569 m a.s.l. where $T = -16\,^{\circ}\mathrm{C}$. As the aircraft descended, LWC increased rapidly to $0.9\,\mathrm{g\,m^{-3}}$ at 30 m below cloud top, the highest LWC recorded at any point during the flight. Mean droplet diameters in this region were ∼ 23 µm in concentrations of $\sim 90\,\mathrm{cm^{-3}}$. 2D-S images revealed many small liquid droplets with a few small (mean diameter 190 µm) irregular ice crystals (Fig. 3a) with $N_{\mathrm{ice}} \sim 1\,\mathrm{L^{-1}}$. The region immediately below this cloud top layer, between 1520 and 1275 m, exhibited a steady decline in LWC while droplet concentrations and N_{ice} maintained similar values to those observed in the cloud top region. Mean ice crystal diameters increased markedly to 520 µm before LWCs eventually fell to below the threshold value ($0.01\,\mathrm{g\,m^{-3}}$), marking the base of an upper layer of cloud. A subsequent cloud layer, 750 m below, was then encountered. In the clear air region separating these two cloud layers temperatures rose by around 5 to −11 °C and large (∼ 760 µm) irregular snow particles, some of which exhibited dendritic growth habits, were observed. Precipitation concentrations were generally $< 0.5\,\mathrm{L^{-1}}$. Mean IWCs in this precipitation zone were $\sim 0.01\,\mathrm{g\,m^{-3}}$. The particles observed falling from the higher cloud layer descended into the cloud layer below at 1275 m a.s.l. In the top of this lower cloud layer ($T = -11\,^{\circ}\mathrm{C}$) LWCs rose to $0.4\,\mathrm{g\,m^{-3}}$ with N_{drop} (mean diameter 15 µm) increasing to $\sim 120\,\mathrm{cm^{-3}}$ while N_{ice} increased to $\sim 1\,\mathrm{L^{-1}}$, 2D-S probe imagery in this region revealed the presence of larger snow particles (mean diameters ∼ 815 µm). As the aircraft descended further, LWCs gradually decreased while N_{drop} remained fairly constant before

ACPD
14, 28757–28807, 2014

reaching cloud base at 280 m, (much closer to sea level than in profiles A1 and A2). Below cloud base precipitating snow (mean particle size ~ 625 µm) was observed.

Appendix B:

B1 Profiled ascent B2

During profiled ascent B2 (prior to profile descent B1 above) the aircraft climbed from below cloud base at 190 m ($T = -5\,^{\circ}C$) travelling initially through snow precipitation in concentrations peaking at $\sim 3\,L^{-1}$ (mean diameter 420 µm). Images revealed dendritic ice crystals that had descended from the cloud layer above (Fig. 5c). IWCs in this region peaked at $0.025\,g\,m^{-3}$. Cloud base during this profile was less well defined than in later ascents with variable LWCs and droplet number concentrations before a more defined cloud base was encountered at 1010 m. N_{drop} then increased rapidly to $270\,cm^{-3}$ (mean diameter ~ 12.5 µm) while LWCs increased more gradually to $\sim 0.4\,g\,m^{-3}$. N_{ice} through this region showed a decline to $< 0.1\,L^{-1}$, and consisted of precipitating snow particles with a mean diameter of 430 µm. Closer to cloud top (1410 m) ice crystal number concentrations increased, to peak values of $\sim 1\,L^{-1}$. Images (Fig. 5b) showed smaller crystals (mean diameter ~ 370 µm) at this higher altitude, with evidence of hexagonal habits and peak values of IWC $\sim 0.04\,g\,m^{-3}$. Droplet concentrations towards cloud top were similar to lower in the cloud, while LWCs increased to $0.6\,g\,m^{-3}$ and mean droplet diameter increased to ~ 15 µm. The coldest temperature reached within the cloud layer was $-18\,^{\circ}C$, but cloud top (at ~ 1530 m) was warmer by $1\,^{\circ}C$. A further increase of $1\,^{\circ}C$ was observed as the aircraft ascended through the inversion layer. The depth of this cloud layer (520 m) was significantly less than that observed during the previous spring case cloud layer penetrations.

ACPD
14, 28757–28807, 2014

B2 Constant altitude runs B3 and B4

During straight and level run (SLR) B3 the aircraft flew below cloud base at 390 m a.s.l. to characterise precipitation. During B3 the aircraft briefly traversed a region of low cloud with high N_{drop} (peaking at $\sim 520\,cm^{-3}$) but generally low LWCs ($< 0.1\,g\,m^{-3}$). These cloud droplets were small (mean diameter $\sim 6\,\mu m$). 2D-S imagery also revealed small drops were present together with snow crystals (mean diameter $\sim 370\,\mu m$) that were precipitating into these brief regions of low cloud. During B3 temperatures increased from -12 to $-10\,^{\circ}C$. Crystal habits in the out of cloud regions were dominated by aggregates of dendrites and some pristine ice crystals ($\sim 0.5\,L^{-1}$). Here, LWCs were below $0.01\,g\,m^{-3}$, although the 2D-S also detected drizzle droplets precipitating from the cloud layer above (mean concentration $\sim 0.2\,L^{-1}$). Later in B3 the aircraft left its constant altitude and descended to 80 m a.s.l. ($T = -8.5\,^{\circ}C$). Mean N_{ice} increased to $\sim 2\,L^{-1}$ with peaks up to $4\,L^{-1}$. There was a corresponding increase in 2D-S droplet concentrations to a mean of $\sim 1\,L^{-1}$. 2D-S imagery shows the presence of small columnar shaped ice crystals (similar to those shown in Fig. 5d), together with larger snow particles and drizzle droplets. CDP LWC was $< 0.01\,g\,m^{-3}$ in this region, since the larger drizzle droplets measured by the 2D-S were outside the CDP size range. In this region of enhanced N_{ice}, just above the sea surface, IWCs, which were generally $< 0.01\,g\,m^{-3}$ in the below cloud base region, increased to peak values of $0.04\,g\,m^{-3}$.

At the start of run B4, prior to undertaking a mainly straight and level run (SLR) initially to the NW, the aircraft first descended from the inversion layer ($T = \sim -14\,^{\circ}C$) into the cloud top (1050 m a.s.l.). LWC initially rose sharply to a peak of $0.5\,g\,m^{-3}$ before gradually falling away to a mean value $\sim 0.3\,g\,m^{-3}$. Mean droplet concentrations over a ~ 5 min period were $340\,cm^{-3}$ (mean diameter 11 µm) and the 2D-S imagery revealed the presence of small droplets together with large snow crystals (mean diameter 730 µm) in concentrations $< 0.1\,L^{-1}$ and IWCs of $0.03\,g\,m^{-3}$. At 12:40 UTC a generally cloud free region was encountered and sampled for ~ 4 min before re-entering cloud again. During this period the aircraft was turned onto a reciprocal heading at the NW

ACPD
14, 28757–28807, 2014

limit of its track. Cloud microphysics measurements revealed this cloud top region to be very similar to the first period during B4. Mean values of LWC over ∼ 4 min period were 0.2 g m^{-3}, droplet concentrations (mean diameter ∼ 9 µm) were ∼ 340 cm^{-3}. N_{ice} while generally less than 1 L^{-1} (IWC ∼ 0.01 g m^{-3}) showed brief increases (during 1 s integration periods) to 2 L^{-1} and IWC values peaked at 0.1 g m^{-3}. 2D-S imagery showed the presence of dendritic ice particles (mean diameter 750 µm) together with small spherical particles, likely to be liquid droplets. Temperatures in the cloud top regions remained fairly constant throughout B4 (between −15 and −16 °C). The aircraft flew above cloud top for the remainder of the SE-bound leg, and found there to be no ice particles falling into cloud top from above.

Appendix C:

C1 Stepped run C1

The BAS aircraft performed a stepped profile (flight segments C1.1–C1.4) from a cloud top altitude of ∼ 3000 m down to 2249 m covering the temperature range −7.5 to −2 °C. In total 4 SLRs and 4 profiled descents were carried out during this run. During the first penetration of cloud (run C1.1), N_{drop} over a 2 min period was 240 cm^{-3}. LWCs rose to ∼ 0.1 g m^3 and the droplet mean diameter was 10.5 µm. N_{ice} was generally very low during this period < 0.25 L^{-1} with some peaks up to 0.5 L^{-1}. During C1.1 the aircraft maintained an altitude of ∼ 3000 m for several minutes. The cloud microphysics remained predominantly stable, with low N_{ice} (< 0.25 L^{-1}) and LWCs ∼ 0.01 g m^{-3}. The only notable change was a slight increase in the mean diameter of droplets measured by the CDP to 11.5 µm and a reduction in number concentration to 185 cm^{-3}. At ∼ 09:00 UTC the aircraft descended ∼ 100 m to start run C1.2 (T = −6 °C), and encountered a cloud sector where N_{ice} increased to 2 L^{-1} with peaks to 5 L^{-1} (and IWC peaks up to 0.03 g m^{-3} observed here). 2D-S imagery (Fig. 7a) revealed irregular ice crystals and the presence of columnar ice both of which appeared to be rimed. Many small

ACPD
14, 28757–28807, 2014

single pixel (10 µm) particles were also measured. These likely represent the small droplets detected by the CDP in this region (mean diameter 13.5 µm) in concentrations of 125 cm^{-3}. Later during C1.2, N_{ice} fell to values < 0.25 L^{-1}. The aircraft performed a profiled descent at the start of C1.3, descending 200 m to ∼ 2720 m (T = −4 °C). During the descent, LWCs and droplet number concentrations fell to near zero values while N_{ice} increased to peak values of 5 L^{-1} (and IWC peaked at 0.02 g m^{-3}). 2D-S images again revealed the presence of small (mean diameter 255 µm) rimed irregular ice crystals and ice crystals of columnar habit. In the temperature range spanned by this cloud, these observations are consistent with the contribution of secondary ice production (SIP) through rime-splintering. During C1.3 further N_{ice} peaks up to 5 L^{-1} consisting of columnar particles and irregular ice crystals were observed (Fig. 7b). The liquid phase of the cloud in this region was much more variable than nearer to cloud top. Increases in peak LWCs to 0.01 g m^{-3} were seen together with an increase in droplet number concentrations to ∼ 150 cm^{-3} (mean diameter 13.5 µm). These occurred between periods where LWC values were near zero and the cloud was predominantly glaciated.

During C1.4 the aircraft descended 300 m to 2450 m (T = −3 °C). During this run the time between peaks in N_{drop} increased, while the highest N_{ice} measured during this science flight were observed (peaking at N_{ice} = 35 L^{-1}). IWCs peaked at 0.2 g m^{-3}, which is significantly greater than values observed elsewhere in this cloud system. 2D-S imagery (Fig. 7c) reveals that these high ice crystal number concentrations were dominated by columns (mean diameter 260 µm), which at times were seen together with small liquid droplets. These observations are consistent with SIP through the H–M process.

ACPD
14, 28757–28807, 2014

Appendix D:

D1 Profiled descent D1

Well into the flight, the BAS aircraft performed a profiled descent from cloud top at 3700 m to 2400 m over the temperature range −5.2 to 3 °C. At cloud top, LWCs rose to a peak of 0.3 g m^{-3}, with peak N_{drop} (mean diameter 12.5 µm) up to 270 cm^{-3}. N_{ice}, initially close to zero, rose to peaks of 6 L^{-1} with IWCs up to 0.1 g m^{-3}. 2D-S images (Fig. 9a) showed columnar ice crystals (mean diameter 350 µm) in this region, together with liquid droplets. At times swift transitions between predominantly liquid and glaciated conditions were observed. At 3500 m (T = −3.5 °C) the CDP stopped measuring significant values of LWC (> 0.01 g m^{-3}) and this appeared to mark a gap region in the cloud layer of approximately 100 m in depth. The 2D-S did detect low N_{ice} in this region. These were generally below < 0.5 L^{-1}. When the aircraft descended into the lower cloud layer (T = −2 °C) LWCs increased to peak values of 1 g m^{-3}, where N_{drop} (mean diameter 13.5 µm) increased to values as high as 250 cm^{-3}. 2D-S imagery revealed few ice crystals in this region but high drizzle drop concentrations.

At 2800 m (T = 0 °C) a further period of drizzle droplets was observed in the 2D-S imagery. These again appeared stretched and made it impossible to separately identify ice in the data set, so there is no reliable ice crystal mass and number concentration data in this region. At this time, CDP LWCs peaked at 0.4 g m^{-3} and droplet concentrations varied from close to zero to up to ∼ 350 cm^{-3}. The mean diameter of the droplets measured by the CDP was 10 µm. As the aircraft descended towards its minimum descent altitude large variations in LWCs and droplet concentrations continued to be observed with peaks up to 0.2 g m^{-3} and 420 cm^{-3} respectively.

ACPD
14, 28757–28807, 2014

References

Baumgardner, D., Jonsson, H., Dawson, W., O'Connor, D., and Newton, R.: The cloud, aerosol and precipitation spectrometer: a new instrument for cloud investigations, Atmos. Res., 59–60, 251–264, doi:10.1016/S0169-8095(01)00119-3, 2001.

Bergeron, T.: On the Physics of Clouds and Precipitation, Proces Verbaux de l'Association de Météorologie, International Union of Geodesy and Geophysics, 156–178, 1935.

Brown, P. and Francis, P.: Improved measurements of the ice water content in cirrus using a total-water probe, J. Atmos. Ocean. Tech., 12, 410–414, 1995.

Callaghan, T. V., Johansson, M., Key, J., Prowse, T., Ananicheva, M., and Klepikov, A.: Feedbacks and interactions: from the Arctic cryosphere to the climate system, Ambio, 40, 75–86, doi:10.1007/s13280-011-0215-8, 2012.

Crosier, J., Bower, K. N., Choularton, T. W., Westbrook, C. D., Connolly, P. J., Cui, Z. Q., Crawford, I. P., Capes, G. L., Coe, H., Dorsey, J. R., Williams, P. I., Illingworth, A. J., Gallagher, M. W., and Blyth, A. M.: Observations of ice multiplication in a weakly convective cell embedded in supercooled mid-level stratus, Atmos. Chem. Phys., 11, 257–273, doi:10.5194/acp-11-257-2011, 2011.

Crosier, J., Choularton, T. W., Westbrook, C. D., Blyth, a. M., Bower, K. N., Connolly, P. J., Dearden, C., Gallagher, M. W., Cui, Z., and Nicol, J. C.: Microphysical properties of cold frontal rainbands, Q. J. Roy. Meteor. Soc., 140, 1257–1268, doi:10.1002/qj.2206, 2013.

Curry, J. A., Rossow, W. B., Randall, D., and Schramm, J. L.: Overview of Arctic cloud and radiation characteristics, J. Climate, 9, 1731–1764, 1996.

Curry, J. A., Pinto, J. O., Benner, T. and Tschudi, M.: Evolution of the cloudy boundary layer during the autumnal freezing of the Beaufort Sea, J. Geophys. Res., 102, 13851–13860, doi:10.1029/96JD03089, 1997.

DeMott, P. J., Prenni, A. J., Liu, X., Kreidenweis, S. M., Petters, M. D., Twohy, C. H., Richardson, M. S., Eidhammer, T., and Rogers, D. C.: Predicting global atmospheric ice nuclei distributions and their impacts on climate, P. Natl. Acad. Sci. USA, 107, 11217–11222, doi:10.1073/pnas.0910818107, 2010.

Field, P. R., Heymsfield, A. J., and Bansemer, A.: Shattering and particle interarrival times measured by optical array probes in ice clouds, J. Atmos. Ocean. Tech., 23, 1357–1371, doi:10.1175/JTECH1922.1, 2006.

ACPD
14, 28757–28807, 2014

Grosvenor, D. P., Choularton, T. W., Lachlan-Cope, T., Gallagher, M. W., Crosier, J., Bower, K. N., Ladkin, R. S., and Dorsey, J. R.: In-situ aircraft observations of ice concentrations within clouds over the Antarctic Peninsula and Larsen Ice Shelf, Atmos. Chem. Phys., 12, 11275–11294, doi:10.5194/acp-12-11275-2012, 2012.

Herman, G. and Goody, R.: Formation and persistence of summertime Arctic stratus clouds, J. Atmos. Sci., 33, 1537–1553, doi:10.1175/1520-0469(1976)033<1537:FAPOSA>2.0.CO;2, 1976.

Hobbs, P. V. and Rangno, A. L.: Microstructures of low and middle-level clouds over the Beaufort Sea, Q. J. Roy. Meteor. Soc., 124, 2035–2071, doi:10.1002/qj.49712455012, 1998.

Intrieri, J. M.: An annual cycle of Arctic surface cloud forcing at SHEBA, J. Geophys. Res., 107, 8039, doi:10.1029/2000JC000439, 2002.

Kahl, J. D.: Characteristics of the low-level temperature inversion along the Alaskan Arctic coast, Int. J. Climatol., 10, 537–548, 1990.

Korolev, A. V., Emery, E. F., Strapp, J. W., Cober, S. G., Isaac, G. A., Wasey, M., and Marcotte, D.: Small ice particles in tropospheric clouds: fact or artifact?, B. Am. Meteorol. Soc., 92, 967–973, doi:10.1175/2010BAMS3141.1, 2011.

Lance, S., Brock, C. A., Rogers, D., and Gordon, J. A.: Water droplet calibration of the Cloud Droplet Probe (CDP) and in-flight performance in liquid, ice and mixed-phase clouds during ARCPAC, Atmos. Meas. Tech., 3, 1683–1706, doi:10.5194/amt-3-1683-2010, 2010.

Lawson, P. R.: The 2D-S (stereo) probe: design and preliminary tests of a new airborne high-speed, high resolution particle imagine probe, J. Atmos. Ocean. Tech., 23, 1462–1477, 2006.

McFarquhar, G. M., Um, J., and Jackson, R.: Small cloud particle shapes in mixed-phase clouds, J. Appl. Meteorol. Clim., 52, 1277–1293, doi:10.1175/JAMC-D-12-0114.1, 2013.

Mcinnes, K. and Curry, J.: Modelling the mean and turbulent structure of the summertime Arctic cloudy boundary layer, Bound.-Lay. Meteorol., 73, 125–143, 1995.

Neiburger, M.: Reflection, absorption, and transmission of insolation by stratus cloud, J. Meteorol., 6.2, 98–104, 1949.

Overland, J. E. and Wang, M.: When will the summer Arctic be nearly sea ice free?, Geophys. Res. Lett., 40, 2097–2101, doi:10.1002/grl.50316, 2013.

Parkinson, C. L. and Comiso, J. C.: On the 2012 record low Arctic sea ice cover: combined impact of preconditioning and an August storm, Geophys. Res. Lett., 40, 1356–1361, doi:10.1002/grl.50349, 2013.

ACPD
14, 28757–28807, 2014

Rosenberg, P. D., Dean, A. R., Williams, P. I., Dorsey, J. R., Minikin, A., Pickering, M. A., and Petzold, A.: Particle sizing calibration with refractive index correction for light scattering optical particle counters and impacts upon PCASP and CDP data collected during the Fennec campaign, Atmos. Meas. Tech., 5, 1147–1163, doi:10.5194/amt-5-1147-2012, 2012.

Tsay, S. and Jayaweera, K.: Physical characteristics of Arctic stratus clouds, J. Clim. Appl. Meteorol., 23, 584–596, 1984.

ACPD

14, 28757–28807, 2014

Table 1. Flight numbers, run numbers, and their associated time intervals, altitude and temperature range for the four ACCACIA case studies presented.

Flight	Run Number	Time (UTC)	Altitude (m)	Temperature (°C)
B761	A1	13:13:26–13:16:43	1850–50	−19 to −5
B761	A2	13:04:40–13:10:33	300–1850	−8 to −19
B761	A3	13:23:20–13:33:19	1700–50	−19 to −7
B768	B1	11:45:16–11:54:02	1600–50	−17 to −9
B768	B2	11:38:39–11:44:59	50–1600	−17 to −4
B768	B3	12:01:30–12:19:08	400–50	−12 to −9
B768	B4	12:32:20–12:48:14	1300–1050	−16 to −14
M191	C1.1	08:53:45–09:00:00	~ 2950	~ −7
M191	C1.2	09:00:00–09:06:50	~ 2900	~ −6
M191	C1.3	09:06:50–09:13:35	~ 2750	~ −5
M191	C1.4	09:13:35–09:21:09	2750–2250	−4 to −2
M191	C2	10:14:58–10:33:51	3350–2300	−7 to −3
M192	D1	12:58:58–13:06:02	3100–3750	−5 to −1
M192	D2	12:19:10–12:48:16	3100–3750	−5 to −1

ACPD
14, 28757–28807, 2014

Table 2. Measurements of: aerosol concentrations > 0.5 µm from the CAS and PCASP probes, together with predicted primary IN number using the DeMott et al. (2010) (D10) scheme (with either CAS or PCASP aerosol concentration data as input). Observed minimum median cloud temperatures were input to D10, and IN predictions were compared with observed maximum median ice concentrations.

Flight	Max Median Ice (L^{-1})	Min Median Temp (°C)	Max RH (%)	CAS Aerosol Conc (cm^{-3})	PCASP Aerosol Conc (cm^{-3})	Predicted CAS IN value (L^{-1})	Predicted PCASP IN value (L^{-1})
Case 1a	0.61	−18.7	90.3	0.99 ± 0.25	3.13 ± 1.74	1.02 ± 1.14/0.88	1.80 ± 2.25/1.20
Case 1b	0.61	−18.7	22.16	0.14 ± 0.1	4.94 ± 2.22	0.38 ± 0.50/0.21	2.26 ± 2.72/1.68
Case 1c	0.61	−18.7	85.43	1.48 ± 0.37	4.04 ± 2.25	1.24 ± 1.34/1.08	2.05 ± 2.55/1.37
Case 2a	0.47	−16.2	69.68	1.50 ± 0.30	3.23 ± 1.68	0.76 ± 0.82/0.69	1.05 ± 1.26/0.77
Case 2b	0.47	−16.2	92.60	2.40 ± 0.32	4.96 ± 2.28	0.93 ± 0.98/0.87	1.27 ± 1.49/097
Case 2c	0.47	−16.2	93.86	2.07 ± 6.57	3.07 ± 1.86	0.87 ± 1.61/	1.03 ± 1.26/0.69
Case 3a	3.35	−10	89.37	0.06 ± 0.07	–	0.06 ± 0.07/	–
Case 3b	3.35	−10	59.66	0.15 ± 0.11	–	0.08 ± 0.09/0.05	–
Case 3c	3.35	−10	89.79	0.33 ± 0.76	–	0.10 ± 0.13/	–
Case 3d	3.35	−10	89.70	0.48 ± 0.21	–	0.11 ± 0.12/0.09	–
Case 4a	2.50	−4.3	79.70	3.73 ± 1.03	–	0.009 ± 0.009/0.009	–
Case 4b	2.50	−4.3	73.46	4.03 ± 0.58	–	0.009 ± 0.009/0.009	–
Case 4c	2.50	−4.3	31.57	0.24 ± 0.14	–	0.007 ± 0.007/0.006	–

ACPD
14, 28757–28807, 2014

Table 3. Table reproduced from Grosvenor et al. (2012) reporting observations of ice number concentrations, aerosol concentrations > 0.5 µm and primary IN predictions using the D10 parameterisation.

Flight	Mean Ice Conc (L^{-1})	Max ± SD (60 s) Ice Conc (L^{-1})	Temp of Max Conc (°C)	Max RH for Aerosol (%)	Observed Aerosol Conc (cm^{-3})	Predicted IN Value (L^{-1})
Cloud Layers Over Larsen C						
99-i4	0.007 ± 0.002	0.017 ± 0.007/0.005	−13.8	50	0.33 ± 0.05	0.25
99-i5	0.007 ± 0.001	0.020 ± 0.007/0.004	−16.5	50	0.33 ± 0.05	0.41
104-i3	0.008 ± 0.002	0.012 ± 0.005/0.003	−17.7	40	0.15 ± 0.03	0.35
104-i4	0.011 ± 0.002	0.032 ± 0.010/0.007	−13.4	60	0.15 ± 0.03	0.17
Hallett Mossop Zone Ice						
100-i1	0.52 ± 0.02	1.28 ± 0.06/0.38	−0.7	75	0.42 ± 0.05	1.9×10^{-5}
100-i2	1.14 ± 0.02	3.44 ± 0.11/1.01	−2.3	75	0.42 ± 0.05	9.1×10^{-4}
100-i3	1.47 ± 0.02	6.26 ± 0.15/1.78	−4.3	75	0.42 ± 0.05	0.007
100-i4	0.90 ± 0.02	4.77 ± 0.12/1.28	−5.9	75	0.42 ± 0.05	0.019
100-i5	0.05 ± 0.01	0.06 ± 0.01/0.01	−5.6	75	0.42 ± 0.05	0.016
100-i6	0.040 ± 0.008	0.07 ± 0.01/0.03	−5.2	75	0.42 ± 0.05	0.013
104-i5	0.098 ± 0.007	0.37 ± 0.03/0.12	−2.3	94	0.1 ± 0.05	8.3×10^{-4}
104-i6	0.33 ± 0.01	2.7 ± 0.01/0.63	−2.3	94	0.1 ± 0.05	8.3×10^{-5}

ACPD
14, 28757–28807, 2014

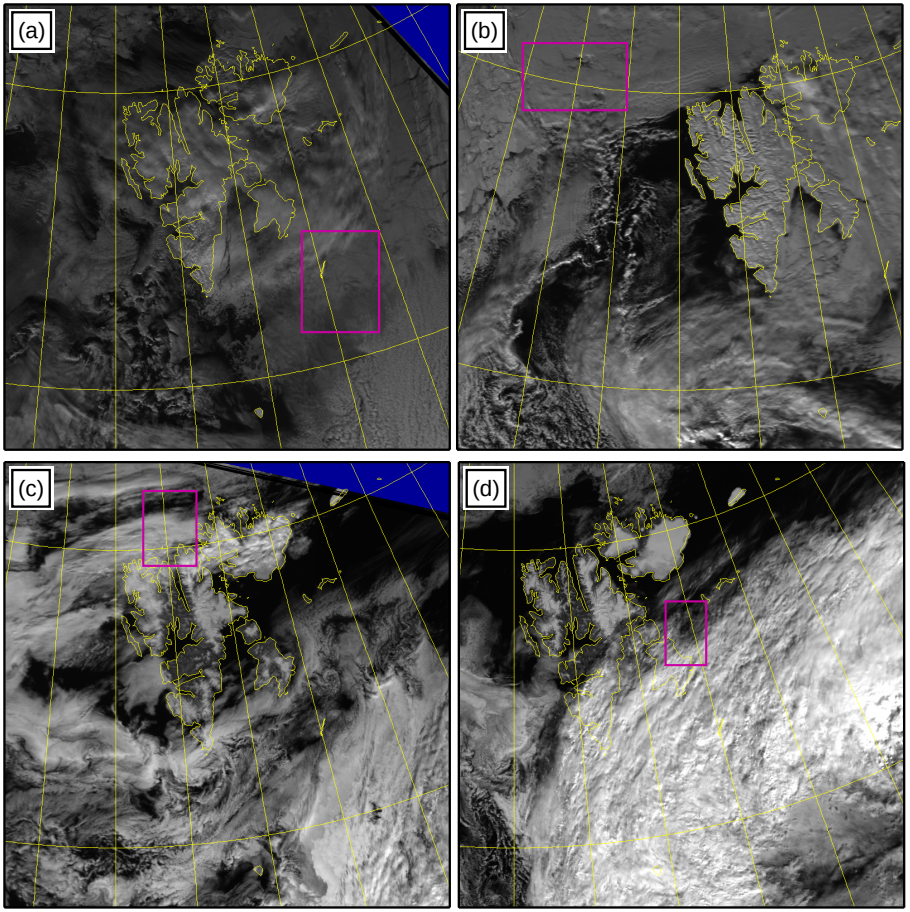

Figure 1. AVHRR visible satellite imagery for spring case 1 **(a)**, spring case 2 **(b)**, summer case 1 **(c)** and summer case 2 **(d)**. Science flight area highlighted by purple boxes in each figure.

ACPD
14, 28757–28807, 2014

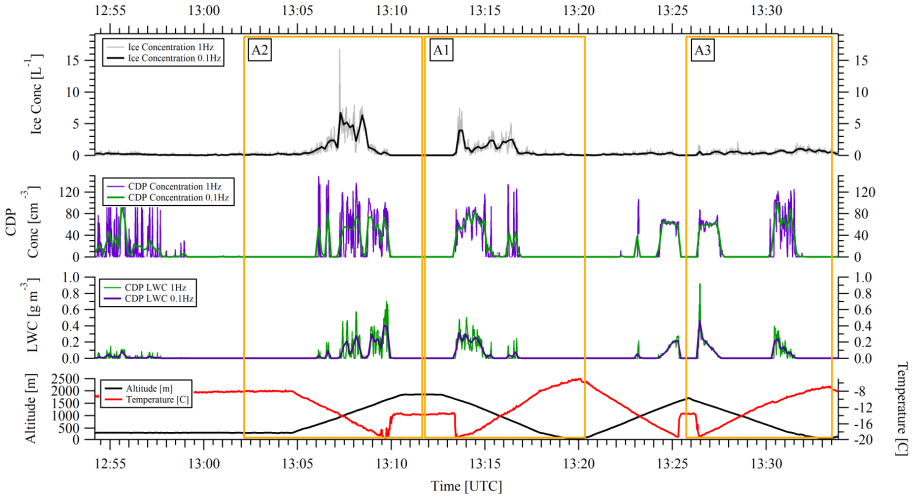

Figure 2. Microphysics time series for spring case 1. Data includes temperature (°C) and altitude (m) (lower panel) together with 1 and 10 s data sets for CDP liquid water content ($g\,m^{-3}$) (panel 2 from bottom), CDP cloud particle number concentration (cm^{-3}) (panel 3), and ice water content ($g\,m^{-3}$) and ice number concentrations (L^{-1}) (top panel). Profiles A2 and A3 are described in Appendix A.

ACPD
14, 28757–28807, 2014

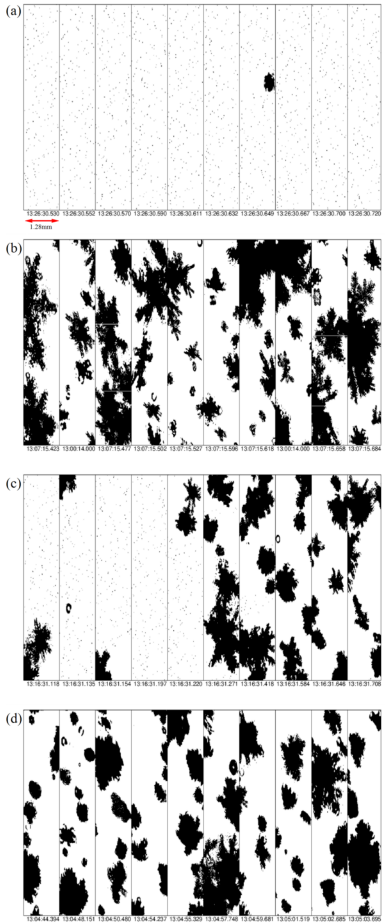

Figure 3. Images from the 2D-S cloud probe during spring case 1 from: (a) a cloud top region during A1; **(b)** 500 m below cloud top during A2; **(c)** region of swift transitions between ice and liquid and **(d)** precipitation region below cloud base.

ACPD
14, 28757–28807, 2014

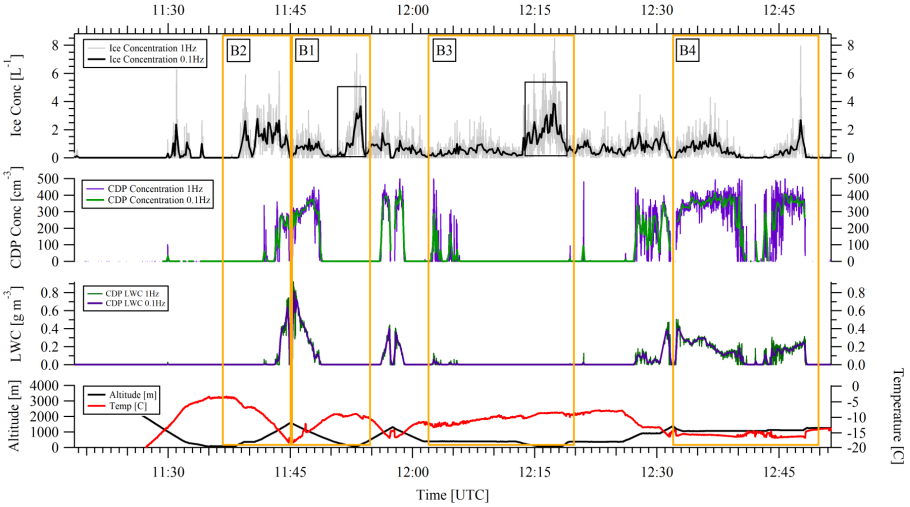

Figure 4. Microphysics time series data for spring case 2. Data includes temperature (°C) and altitude (m) (lower panel) 1 and 10 s data sets for CDP liquid water content ($g\,m^{-3}$) and CDP concentration (cm^{-3}) (middle panels), and ice water content ($g\,m^{-3}$) and ice number concentrations (L^{-1}) (top panel). Profiles B2, B3 and B4 are described in Appendix B.

ACPD
14, 28757–28807, 2014

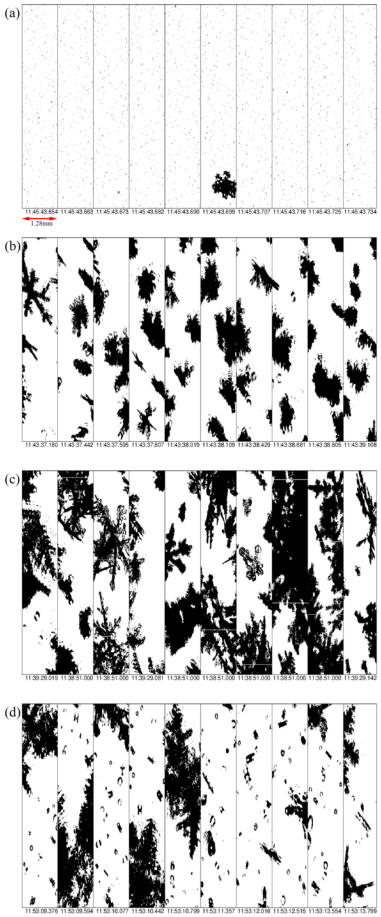

Figure 5. Images from the 2D-S cloud probe from spring case 2 for: **(a)** cloud top during B1; **(b)** profiled ascent during B2; **(c)** dendritc ice in the cloud base region during B2 and **(d)** columnar ice above the sea surface during B2.

ACPD
14, 28757–28807, 2014

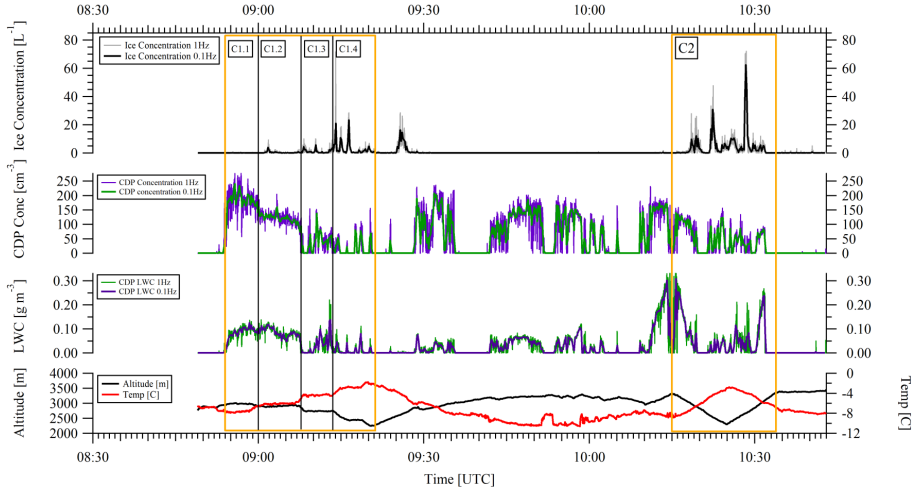

Figure 6. Microphysics time series data for summer case 1. Data includes temperature (°C), altitude (m) (lower panel) together with 1 and 10 s data sets for CDP liquid water content (g m^{-3}) (second panel up), CDP concentration (cm^{-3}), ice water content (g m^{-3}) and ice number concentrations (L^{-1}) (top panel). Flight segments C1.1, C1.2, C1.3 and C1.4 are described in Appendix C.

ACPD
14, 28757–28807, 2014

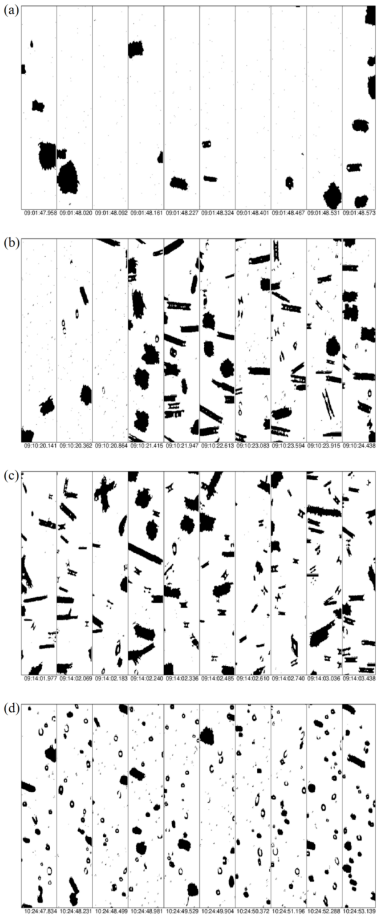

Figure 7. Images from the 2D-S cloud probe from summer case 1 for: **(a)** small irregular ice during C1.2; **(b)** and **(c)** secondary ice production during C1.3 and C1.4 respectively, and **(d)** ice together with drizzle during C2.

ACPD
14, 28757–28807, 2014

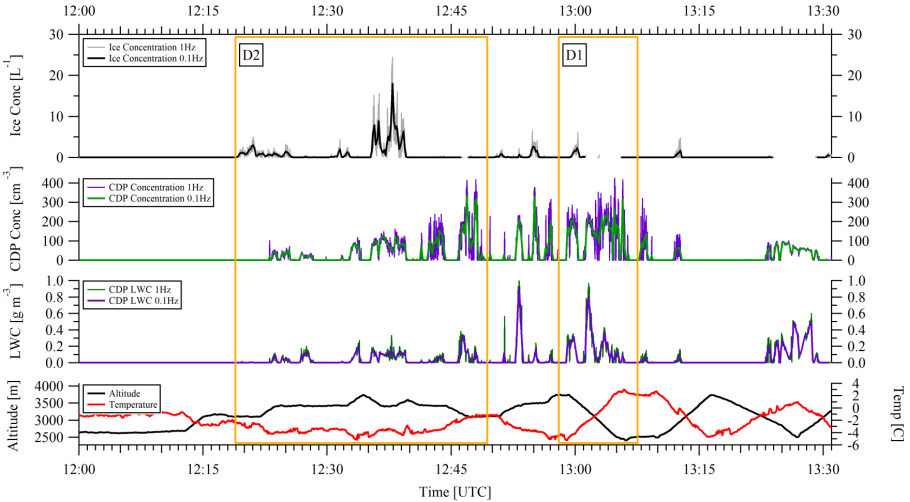

Figure 8. Microphysics time series data for summer case 2. Data includes temperature (°C), altitude (m) (lower panel) together with 1 and 10 s data sets for CDP liquid water content (g m^{-3}), CDP concentration (cm^{-3}) (middle panels), ice water content (g m^{-3}) and ice number concentrations (L^{-1}) (top panels). Profile D1 is described in Appendix D.

ACPD
14, 28757–28807, 2014

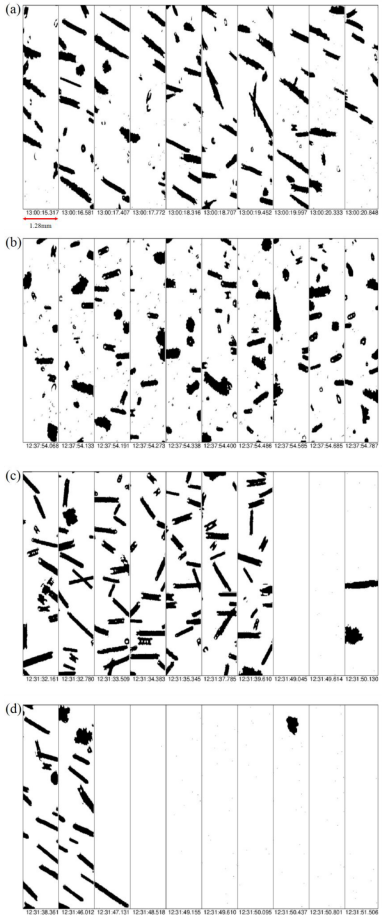

Figure 9. 2D-S cloud probe imagery for summer case 2 showing: **(a)** columnar ice during D1; **(b)** images of columns together with liquid during D2 and swift transitions between **(c)** glaciated and **(d)** liquid phases during D2.

ACPD
14, 28757–28807, 2014

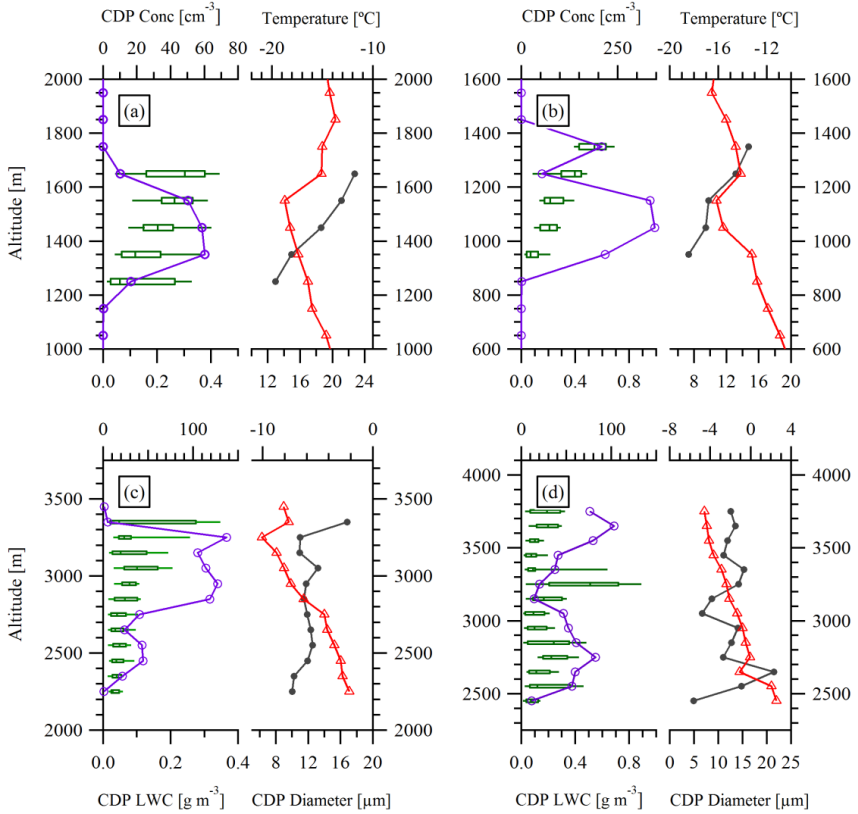

Figure 10. Percentile plots (50th, 25th, 75th percentiles, whiskers to 10 and 90 %) as a function of altitude for LWC from CDP (green), and median droplet number concentration (purple), median droplet diameter (grey) and median temperature (red). Data are averaged over 100 m deep layers. **(a–d)** are for Spring Case 1, Spring Case 2, Summer Case 1 and Summer Case 2 respectively.

ACPD
14, 28757–28807, 2014

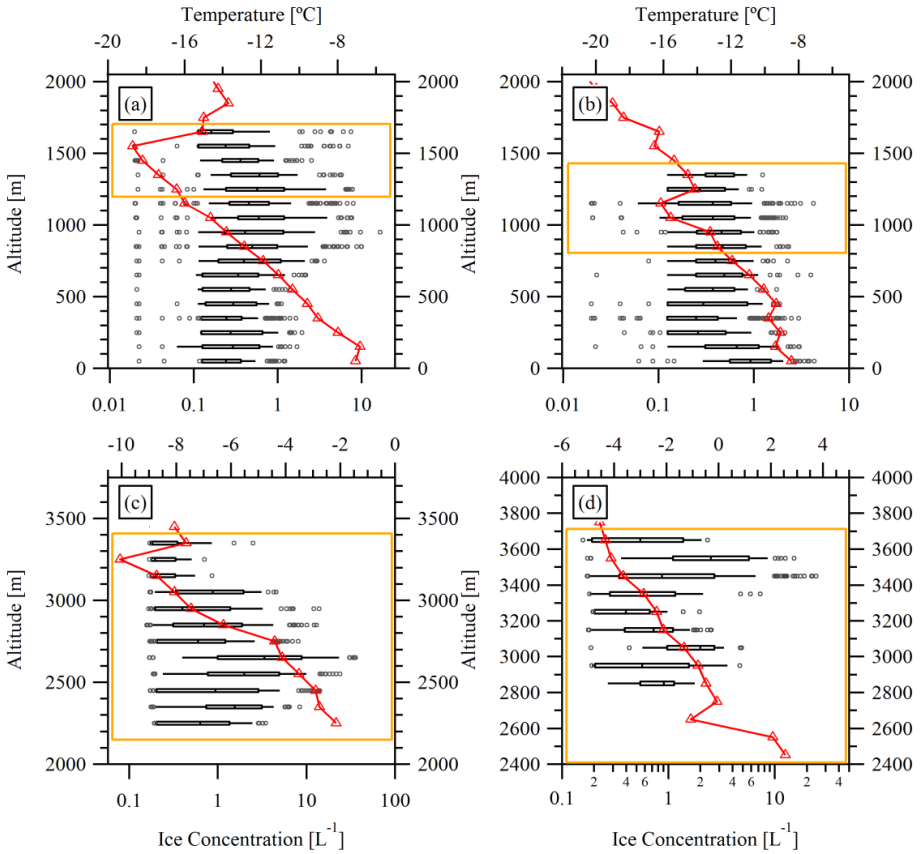

Figure 11. Box and whisker plots with 50th, 25th, 75th percentiles, whiskers to 10 and 90 % and outliers between 95 and 100 % as a function of altitude for ice number concentrations (black) and median temperature (red) (**a**–**d** and altitude averages as in Fig. 10 above). The box in yellow provides an indication of the full extent of cloud layers investigated. **(a–d)** are for Spring Case 1, Spring Case 2, Summer Case 1 and Summer Case 2 respectively.

ACPD
14, 28757–28807, 2014

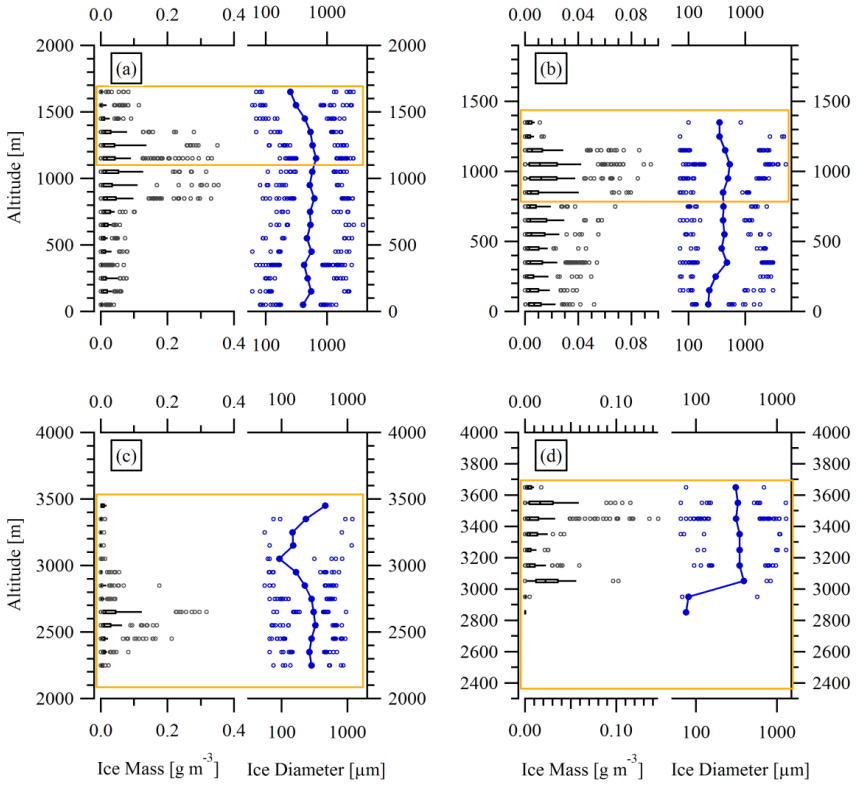

Figure 12. Box and whisker plots with 50th, 25th, 75th percentiles, whiskers to 10 and 90 % and outliers between 95 and 100 % as a function of altitude for ice mass (black) and median ice crystal diameter with outliers between 95 and 100 % (blue). (**a**–**d** and altitude averages as in Fig. 10 above). The box in yellow provides an indication of the full extent of cloud layers investigated. **(a–d)** are for Spring Case 1, Spring Case 2, Summer Case 1 and Summer Case 2 respectively.

ACPD
14, 28757–28807, 2014